JOURNAL OF PROPULSION AND POWER
Vol. 24, No. 5, September–October 2008

Parametric Study of Injection Angle Effects on Stability of Transonic Axial Compressors

H. Khaleghi*
Amirkabir University of Technology, 15875-4413 Tehran, Iran
J. A. Teixeira†
Cranfield University, Cranfield, England MK43 0AL, United Kingdom
and
A. M. Tousi‡ and M. Boroomand§
Amirkabir University of Technology, 15875-4413 Tehran, Iran

DOI: 10.2514/1.34817

An effective approach in suppressing stall is mass injection upstream of the tip of an axial flow compressor. Developing reliable injection systems for high pressure ratio compressors requires an understanding of the effects of injection parameters, for example, injection angle, on the compressor stability and performance. This paper reports on a numerical investigation of injection angle on the operability of a high-speed compressor rotor. The injection port is set to be choked for all of the injection cases. Simulations indicate that injection angle has a significant impact on stability improvement. Maximum range extension is obtained when an injection yaw angle equal to −30 deg is applied. At this injection angle, the stalling mass flow coefficient was reduced by 17.4% by using an injected mass flow equivalent to 1.55% of the baseline annulus flow. Results also indicate that the best injection case creates an incidence angle of about 0 deg over the tip of the blade and adds the highest momentum in the relative frame of reference.

Nomenclature

A	=	area
a	=	annulus
adb	=	adiabatic
amb	=	ambient
DF	=	diffusion factor
in	=	blade inlet
j	=	jet
out	=	blade outlet
P_0	=	total pressure
rel	=	relative frame of reference
T_0	=	total temperature
t	=	tip
U, V	=	velocity
x	=	axial component
y^+	=	nondimensional wall distance
η	=	efficiency
θ	=	tangential component
μ	=	momentum
ρ	=	density
σ	=	solidity
ϕ	=	flow coefficient

Received 26 September 2007; revision received 20 May 2008; accepted for publication 19 June 2008.

*Doctoral Student, Aerospace Engineering Department: khaleghi@aut.ac.ir. Student Member AIAA.
†Lecturer, Department of Power and Propulsion, School of Engineering; j.a.amaral.teixeira@cranfield.ac.uk.
‡Associate Professor, Aerospace Engineering Department; tousi@aut.ac.ir.
§Associate Professor, Aerospace Engineering Department; boromand@aut.ac.ir. Member AIAA.

I. Introduction

THE operating range of axial flow compressors is generally limited by the onset of aerodynamic instabilities, surge, and rotating stall. Several researchers have reported that the tip leakage flow has major effects on the instabilities leading to stall inception [1–4]. In transonic compressors, the interaction between the passage shock and the tip leakage vortex creates a region of low-speed fluid just downstream of the interaction [5]. The features of the shock-vortex interaction were investigated by a number of researchers (e.g., Adamczyk et al. [6], Puterbaugh and Brendel [7], and Hah et al. [8]). The unsteadiness and shock motion were studied experimentally and numerically by Copenhaver et al. [9], whose study indicated the presence of deterministic unsteadiness near the location of the shock.

Some approaches to controlling the tip leakage flow and improving the compressor stability, known as casing treatment, used slots and grooves placed in the shroud over the tip of the blade [10–13]. Recirculation casing treatment employs a passageway to remove high-pressure fluid from downstream of the rotor leading or trailing edge and inject it upstream of the point of removal [14–16]. Active control strategies have also been used to suppress the instabilities. Epstein et al. [17] proposed a strategy for extending the stable flow range of compression systems by suppressing rotating stall and surge using dynamic feedback. A successful attempt to extend the stable flow range of an axial flow compressor was carried out by Day [18]. Adjustable stator blades [19], controllable inlet guide vanes [20], and downstream bleeding [21–23] were also investigated by a number of researchers. Spakovszky et al. [24], Weigl et al. [25], Koch and Smith [26], Lee and Greitzer [27], Suder et al. [28], Stein et al. [29], Hendricks and Gysling [30], and Buhr et al. [31] studied the effect of steady and unsteady tip injection.

Suder et al. [28] investigated, experimentally and numerically, the stability enhancement using discrete tip injection in a high-speed axial compressor rotor. The casing-mounted injectors were located 200% of the rotor axial tip chord upstream of the rotor. The injectors penetrated 5.1 mm from the casing into the flowfield. They showed that range extension is correlated with the increase in mass-averaged axial velocity at the tip due to injection. The maximum range extension was achieved with choked injectors. They also found that the range extension is related to the total circumferential extent of injection. Weigl et al. [25] demonstrated that unsteady injection can be used to recover from a fully developed stall pattern. Results

indicated that the stability improvement using unsteady injection is slightly higher than that obtained with steady injection. Therefore, the total stability enhancement is mostly due to steady injection. Recently, a number of numerical simulations have been reported that study the impact of tip injection on stability improvement [32–34]. Regarding the numerical and experimental studies in the literature, the parametric studies dealing with injection angle variation are few in number.

The objective of this research is to determine the effects of injection angle on the rotor stability and performance. The test case is a high-speed axial flow compressor rotor, NASA Rotor-67. The three-dimensional computational fluid dynamics (CFD) code, CFX 10.0, has been employed to numerically solve the compressible Navier–Stokes equations. The injector size and location have been chosen with the expectation of an improvement in the compressor stability by using a small amount of injected air. A parametric study of tip injection angle on the compressor stability is undertaken. Various injection yaw and pitch angles are applied, and their effects on the compressor stability are investigated.

II. Geometry

The numerical simulations have been performed on a NASA Rotor-67, which is a transonic axial flow compressor rotor [35]. Representative values for this rotor are given in Table 1. To investigate the effect of tip injection on the stability of the current rotor, an annular injector is set up around the whole annulus at about 50% of the rotor axial tip chord upstream of the rotor. The injector penetrates 0.99 mm into the flowfield. Thus, the injector is located radially between the tip of the blade and the shroud. A modified casing is used to treat the injection port as an inlet boundary [36]. The injector configuration is presented in Fig. 1. The injector used in this work is similar in character to the sheet injector used by Weigl et al. [25]. Such an injector injects high-momentum air in the axial direction along the casing wall into the tip region of the compressor.

III. Numerical Method

The flow region close to the blade was discretized using an O-type grid, whereas the outer part was meshed using an H-type grid. The grid consists of 211 nodes in the streamwise, 65 nodes in the spanwise, and 43 nodes in the blade-to-blade direction. Fifteen nodes are used in radial direction to describe the tip clearance gap. The overall grid used in the computations includes 589,745 nodes. Figure 2 shows the blade-to-blade and meridional views of the mesh. The grid clustering near wall surfaces satisfies the $y+$ wall coordinate requirements of the turbulence model while providing an adequate description of the local gradients of the flow. In the present study, a two-equation κ–ε turbulence model is used. A scalable wall function is employed, allowing a consistent grid refinement independent of the Reynolds number. The applied boundary conditions are as follows. At the inlet boundary, the total pressure, total temperature, and flow angle are imposed. At the outlet, the average static pressure integrated over the entire outlet boundary is specified. The walls are considered to be smooth and adiabatic.

Table 1 NASA Rotor-67 design parameters

Characteristic	Value
Number of blades	22
Design rotational speed, rpm	16,043
Tip speed, m/s	429
Inlet tip relative Mach number	1.38
Design mass flow rate, Kg/s	33.25
Design pressure ratio	1.63
Design tip clearance, mm	1.01
Average aspect ratio	1.56
Tip solidity	1.29
Hub solidity	3.11
Inlet hub/tip radius ratio	0.375
Exit hub/tip radius ratio	0.478

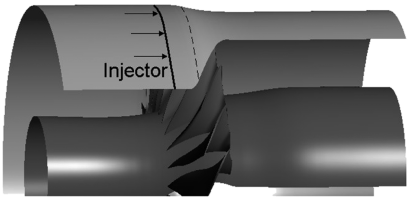

Fig. 1 Injector configuration.

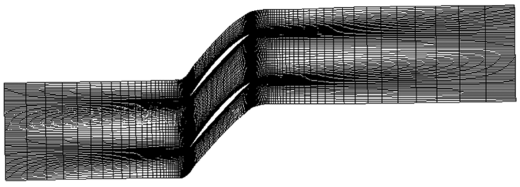

a) Blade-to-blade view

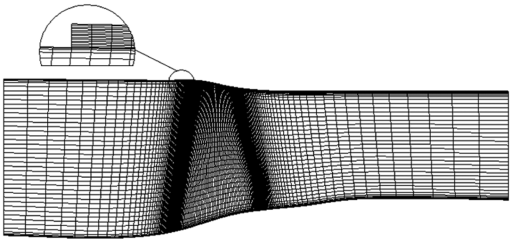

b) Meridional view

Fig. 2 Computational grid.

Periodic boundary conditions are used for the single passage domain. At the injection port, the velocity components and total temperature are specified. Compression of the injected air results in an increase in the total temperature. The total temperature of the fluid injected in this work is higher than that of the flow entering the compressor passage. An approximate temperature rise of 32° was calculated by assuming isentropic compression. This causes the calculation to be more realistic because in real applications the injected air is taken from downstream of the compressor and the ensuing increase in the total temperature at the casing results in an efficiency drop. Because the absolute velocity and total temperature are held constant, the total pressure of the injected fluid increases from choke to stall operating conditions for each case, due to an increase in the static pressure near the injection port. An increase in the injection total pressure occurs in real applications in which the injector is supplied by the downstream flow. All the numerical simulations were started from the choking condition and then marched toward the stall point by a gradual increase in the average back pressure. The near-stall condition is judged to be the last stable operating point before the onset of oscillations of the flow parameters that characterize divergence of the solution.

Unsteady events such as shock motion and vortex shedding are clearly not modeled by steady calculations, which will lead to some inaccuracy in the prediction of the stall point. However, a number of researchers have conducted satisfactory steady simulations covering the entire fan characteristic up to near-stall conditions, including Puterbaugh and Brendel [7], Chima [37], and Hah and Reid [38], who dealt with the rotor employed in the present study. To explore the effects of unsteadiness in the current study, transient calculations were performed for the smooth casing and one of the injection cases. A time step of $1e-6$ s was used for the unsteady simulations.

IV. Results and Discussion

The numerical simulations for the smooth casing were validated against the experimental data in the previous publications of the present authors [36,39]. Results showed a satisfactory prediction of the compressor overall performance and flow characteristics. The

Table 2 Injection angles

Configuration	Angle, deg
Pitch angle	4, 7, 15
Positive yaw angle	7, 15, 30
Negative yaw angle (opposite direction of the blade rotation)	−7, −15, −22, −30, −37, −41, −45

grid independence of the computations was checked by using a refined grid. It was also shown that the modified casing does not, by itself, change the overall characteristics and flowfield of the rotor.

To investigate the effect of the injection angle on the stability of Rotor-67, numerical simulations for various injection angles were performed. In the current study, the injector is set to be choked for maximum range extension and to ensure that the injection velocity is identical in all cases, leaving the injection angle as the main variable. Three pitch and 10 yaw angles together with the axial injection were simulated. Table 2 presents the angles applied to the injector. By convention, the negative angles in Table 2 are those whose direction is opposite that of the rotation of the blade. All the angles are measured relative to the axial direction.

Figures 3 and 4 present the overall effect of the injection angle on the compressor characteristic curves of the total pressure ratio and adiabatic efficiency. In these plots, the mass flow rate (sum of the annulus and injected mass flows) is normalized by the corresponding choking mass flow. For the sake of clarity, only the results for the axial injection case are presented in Fig. 3. The calculation of adiabatic efficiency based on Eq. (1), η_{adb}, does not address the issue of the additional work required by the injection process. Therefore, because the injector is supplied by an external source, the work done on the injected air needs to be considered when calculating the overall efficiency. The adiabatic efficiency including the extra work, η'_{adb}, is thus calculated using Eq. (2). Although the injection rate is only a few percent of the main passage flow rate, the effect of the tip injection on the range extension is significant. In addition, the tip injection applied in this work does not change the shape of the compressor characteristics when compared with the datum configuration. Nevertheless the efficiency penalty imposed to the compressor by considering the extra work done on the injected fluid is approximately 1%. Figure 4 shows plots of the normalized mass flow rate and the adiabatic efficiency, calculated from Eq. (2), for the near-stall point of each injection case as a function of the injection angle. This figure demonstrates that injection with either a pitch or positive yaw angle lowers the stability through a rise in the stalling mass flow when compared with the axial injection case. In contrast, a negative yaw angle of less than 30 deg is beneficial to the compressor stability as it increases the operational flow range.

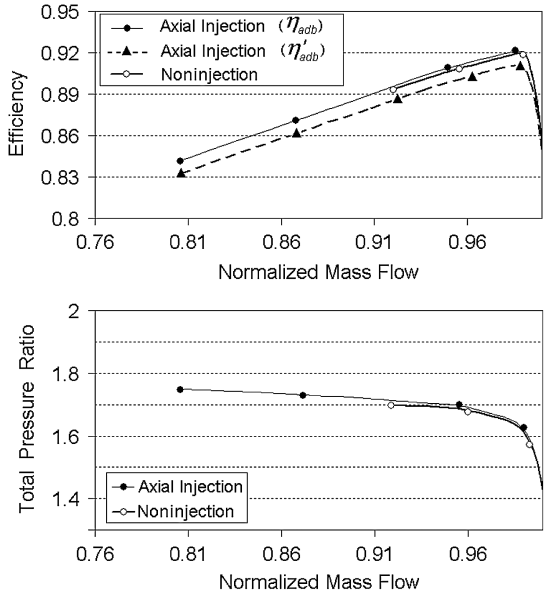

Fig. 3 Impact of axial injection on the compressor characteristics.

$$\eta_{\text{adb}} = \frac{(\frac{P_{02}}{P_{01}})^{\gamma-1/\gamma} - 1}{(\frac{T_{02}}{T_{01}} - 1)} \tag{1}$$

$$\eta'_{\text{adb}} = \frac{(\frac{P_{02}}{P_{01}})^{\gamma-1/\gamma} - 1}{(\frac{T_{02}}{T_{01}} - 1) + \frac{\dot{m}_j}{\dot{m}_{\text{out}}} \times ((\frac{P_{0j}}{P_{\text{amb}}})^{\gamma-1/\gamma} - 1)} \tag{2}$$

The stall margin, which is used to measure the stable operating range of a compressor, is typically defined as the change in mass flow and pressure rise between the operating line and the stall line at a fixed rotational speed. However, an isolated rotor in a compressor rig test does not have an operating line [28]. Therefore, the normalized change in the stalling flow coefficient, defined by Suder et al. [28], is used in this work to measure the operating range extension. This parameter is defined as follows:

$$\Delta\phi_{\text{stall}} = ((\phi_{\text{stall}})_{\text{noninjection}} - (\phi_{\text{stall}}))/(\phi_{\text{stall}})_{\text{noninjection}} \tag{3}$$

The percentage change in the corrected stalling flow rate can be used instead of this parameter because

$$\phi = V_x/U_t = \dot{m}/(\rho U_t A_a) \tag{4}$$

As shown in Fig. 4, the injection angle has a significant impact on the compressor stability. It can be concluded that the incidence over the tip of the blade is related to the range extension. Figure 5a shows the range extension as a function of incidence angles, calculated based on circumferential averaging near the tip of the blade and at the near-stall point of each case. The corresponding incidence for the smooth casing was measured to be about 14 deg. In this plot, the numbers associated with each data point identify the injection angles. As illustrated, maximum range extension is obtained when the incidence due to injection is near 0 deg. The data plotted in Fig. 5a follows two distinct trends: there is a peaked curve describing the

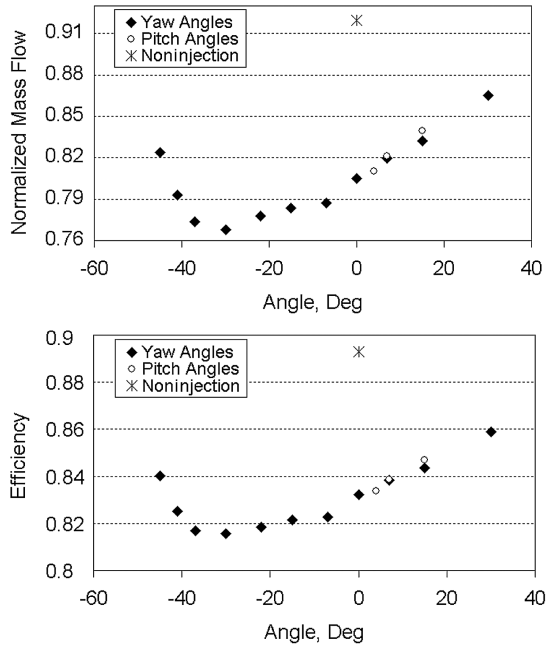

Fig. 4 Effect of injection angle on the near-stall efficiency and normalized mass flow.

range extension vs the yaw angle variation and a quasi-straight line relating pitch injection and range extension. In the first of these curves, the incidence variation corresponding to the injection yaw angles appears to have a strong relation to the range extension. Two factors contribute to the form of this plot: the variation in incidence and the fact that the injected mass flow rate does not remain constant when changing the injection angle. The incidence variation for the case of pitch angles is basically different from that of the yaw angles. The reduction in the incidence angle, which occurs by applying an injection pitch angle, is due to a reduction in the axial velocity caused by the Coanda effect, which will be discussed later.

Figure 5b presents the stable range extension as a function of the injected mass flow normalized by the stalling mass flow rate of the noninjection case. Because the injection area is identical for all cases, applying an injection angle results in a decrement of the injected mass flow. Figure 5b shows that, with the same injection angles, the injected mass flow rates are identical for positive and negative yaw angles. However, the injection pitch angle cases introduce considerably lower injected mass flows compared with the yaw angle cases while having identical injection angles, 7 and 15 deg. This occurs due to the aforementioned Coanda effect. As can be seen in Fig. 5b, injection with a pitch angle (PA) or positive yaw angle (YA) reduces the compressor stable range extension. Small values of PA (less than 5 deg) show a small penalty in terms of compressor stability with respect to the axial injection case. However, higher injection pitch angles are not recommended. It is further shown in Fig. 5b that injection cases with a negative yaw angle less than 30 deg increase the stability. The stalling mass flow coefficient is reduced by 17.4% for injection with the YA equal to −30 deg case. Such injection benefits the stability by 32% when compared with axial injection. The injected mass flow rate for the best injection is 1.55% of the stalling mass flow for the noninjection case. This flow rate is 14% lower than the corresponding value for the axial injection.

Finding a parameter that controls the range extension is desired. Results obtained in [28] indicate that the range extension is related to an increase in the circumferential mass-averaged axial velocity at the tip due to injection. In the present study, the injection port is choked for all the cases. Therefore, stability variation can not be related to the axial velocity because the average axial velocity of the injected fluid decreases by applying an injection angle. The injected mass flow rate corresponding to the best injection case is shown to be lower than that of the axial injection, implying that the injected mass flow or absolute momentum are not correlated to range extension either. The injected velocity in the relative frame of reference increases as a negative YA is applied. However, it can not be related to range extension because the maximum relative velocity is due to injection with a YA equivalent to −45 deg. Range extension can possibly be related to the increase in the momentum in the relative frame of reference, which is defined as follows:

$$\Delta\mu_{\text{rel}} = \frac{(\bar{V}_{j_{\text{rel}}} - \bar{V}_{\text{smooth}_{\text{rel}}} \cos\gamma)}{\bar{V}_{\text{smooth}_{\text{rel}}} \cos\gamma} \times \frac{\dot{m}_j}{\dot{m}_{\text{stall}}} \tag{5}$$

The velocities are calculated based on circumferential averaging in the relative frame of reference. It should be noted that γ is defined as the angle between the relative velocities corresponding to the smooth casing and injection cases. Figure 6 provides a schematic view showing the relationship between the relative velocities used in Eq. (5). The stability improvement as a function of added relative momentum is shown in Fig. 5c. The added momentum due to mass injection appears to have a close relation to the range extension, providing an almost linear relationship.

The effect of tip injection on stability improvement can be better understood by determining the blade loading variations. Suder et al. [28] reported that tip injection increases the stability margin by unloading the tip region of the blade. It was also shown in that work that the blade stalls with or without injection at a critical tip diffusion factor. To understand the effect of the injection angle on the blade loading for the current rotor, the diffusion factors are determined along the span by circumferentially averaging the relative velocities:

$$\text{DF} = 1 - \left(\frac{\bar{V}_{\text{out}}}{\bar{V}_{\text{in}}}\right) + \left(\frac{\Delta\bar{V}_{\theta}}{2\sigma\bar{V}_{\text{in}}}\right) \tag{6}$$

A comparison between the radial distributions of the diffusion factors for the smooth casing and four injection cases, all taken at the near-stalling mass flow of the smooth casing, is presented in Fig. 7a. In the following plot, Fig. 7b, the same cases are plotted at their respective near-stall points. In Fig. 7a, in which the normalized mass flows are the same, the diffusion factors are essentially identical over much of the span. The tip injection reduces the blade loading in the

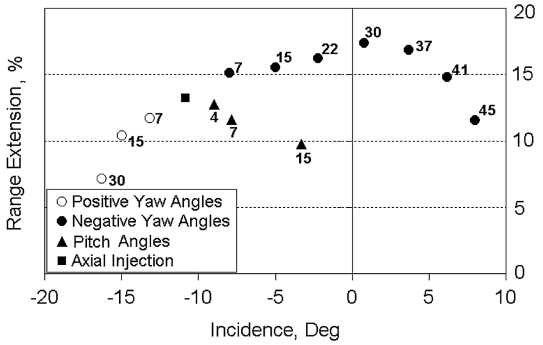

a) Range extension vs incidence angle near the tip

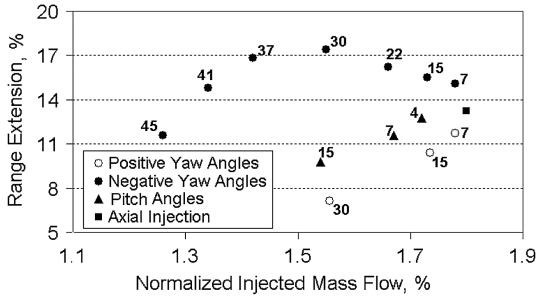

b) Range extension vs normalized injected mass flow

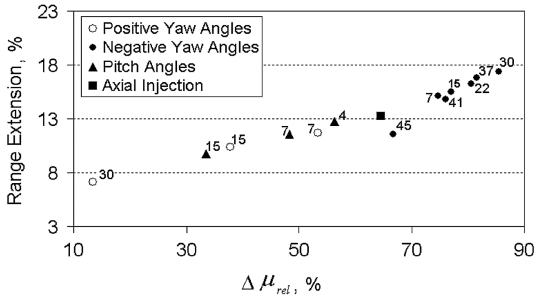

c) Range extension vs added momentum

Fig. 5 Range extension as a function of incidence angle, normalized injected mass flow, and added momentum in the relative frame of reference.

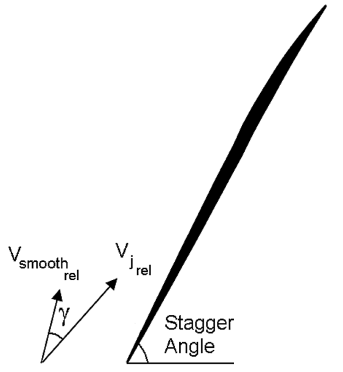

Fig. 6 Relation of the relative velocities used in Eq. (5).

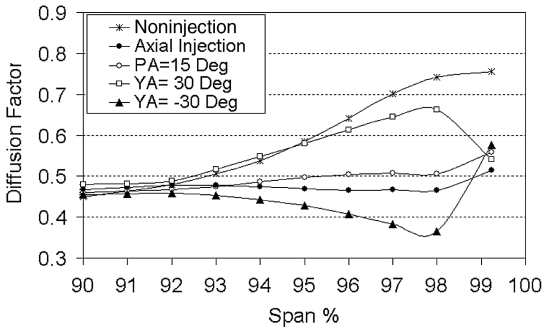

a) At the near-stall condition of the smooth casing

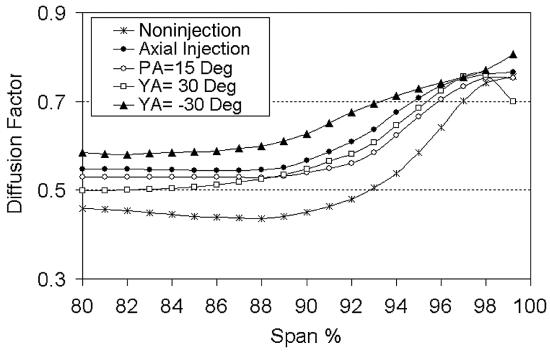

b) At the near-stall condition of each case

Fig. 7 Spanwise distribution of diffusion factors.

tip region and consequently allows the compressor to operate at lower mass flows. It is further shown in this plot that the greatest change in the blade loading occurs at about 98% span. The most effective injection (injection YA equal to −30 deg) results in the lowest blade loading at this location although it increases the blade loading at the tip when compared with the axial injection. As shown in Fig. 7a, injection with a PA or positive YA results in higher blade loading in the tip region as compared with the axial injection, particularly at 98% span. In Fig. 7b, the diffusion factors are not identical over the span due to different operating conditions. This plot suggests that stall occurs when the diffusion factor at 98% span exceeds a value of about 0.75 regardless of the injection configuration (confirming the previous report) [28].

It was demonstrated in Fig. 5b that the injector effectiveness is reduced by applying an injection pitch angle. It was also found that, for the same value of injection angle, the injected mass flow rate is lower for the case of pitch as compared with yaw angles. To explain these findings, the contours of static pressure together with the absolute velocity vectors are given at the near-stall condition of the smooth casing and on the periodic surface in Fig. 8 for three cases. The static pressures are normalized by the ambient pressure. For the sake of clarity, only the part near the injection face is shown. The configurations presented are the smooth casing, the axial injection, and the injection PA of 15 deg. Comparing the two injection cases shows that the static pressure around the injection face drops substantially for the pitch angle case when compared with the axial injection, resulting in the presence of a low-pressure region near the casing. The reason for this behavior relies on the phenomenon known as the Coanda effect. The Coanda effect describes the tendency of a fluid to follow the convex curvature of a solid boundary. It occurs because of a reduction of surface pressure due to a vortex action as the flow passes over the boundary. The same behavior can be observed for the injection with pitch angle case. Figure 8c shows that the injected air follows the solid boundary resulting in lower pressure at the injection face. The injection total pressure also decreases as compared with the axial injection, owing to the lower static pressure. The velocity profiles of the injected fluid in this plot are noticeably different from those corresponding to the axial injection case in Fig. 8b. This difference is due to the presence of a vortical structure induced by the injection of the flow at a pitch angle.

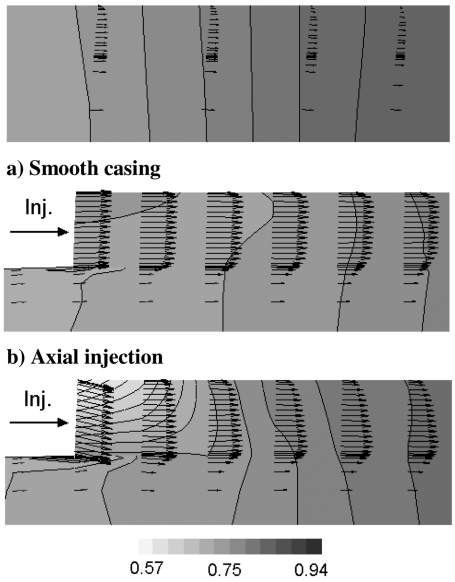

a) Smooth casing

b) Axial injection

c) Injection PA = 15 deg

Fig. 8 Static pressure contours on the periodic surface near the injection face at the near-stall condition of the smooth casing.

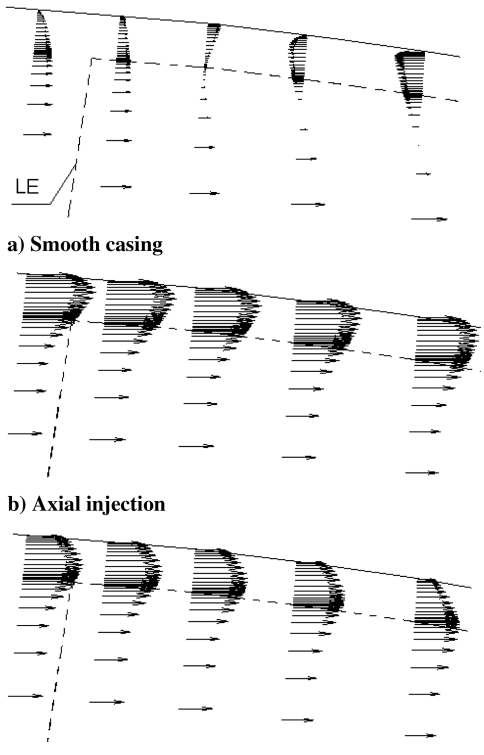

a) Smooth casing

b) Axial injection

c) Injection PA = 15 deg

Fig. 9 Meridional view of the axial velocity vectors on the periodic surface near the blade leading edge.

Figure 9 shows a meridional view of the axial velocity vectors plotted on the periodic surface (middle of the passage) at the mass flow corresponding to the near-stall condition of the smooth casing. Three configurations are shown: the smooth casing, the axial injection, and the injection PA of 15 deg. The position of the blade is specified by dashed lines. The case without injection shows a significantly lower near-casing velocity when compared with the two cases with injection. Between these, there are also significant differences in terms of the local velocity vectors. The injection pitch angle case shows a relatively lower axial velocity over the tip. The profiles of the axial velocity that correspond to the blade leading-

edge locus differ in terms of the location of the peak. In the axial injection case, Fig. 9b, the largest velocity vector is found much closer to the wall when compared with the PA case, Fig. 9c. Further downstream, the velocity profiles appear to be more stable for the axial injection as compared to the injection PA case.

The static pressure contours together with the relative velocity vectors are presented on a surface at 99.6% span in Fig. 10 for four cases. The normalized mass flow rates for these cases correspond to that of the smooth casing at the near-stall point. The configurations presented are the smooth casing, the axial injection, the injection YA of −30 deg, and the injection YA of −45 deg. The solid (bold) lines denote zero axial velocity contour levels whereas the dashed lines specify the blade stagger line. These lines are added to the figure to enable a better comparison between the relative flow angles. The shock position can be inferred from the static pressure contours. A common observation in all the plots refers to the change in direction of the tip gap flow. The passage shock reduces only the velocity component of the clearance flow, which is normal to the shock front. As a result, the relative flow angle increases immediately downstream of the shock, which can be observed from the vectors that are located just after the shock. However, the mainstream flow turns the leakage flow to the streamwise direction further downstream of the shock. As illustrated in Fig. 10a, the noninjection case has a high relative flow angle near the leading edge. In addition, large zones of negative axial velocity fluid are observed downstream of the shock and also near the trailing edge of the blade. The plots for the injection cases, Figs. 10b–10d, all show that the injection of high-velocity air into the tip of the blade decreases the incidence significantly. It is further shown in these figures that the shock is pushed backward in the passage and that the size of the negative axial velocity zone is considerably reduced due to injection. As discussed earlier, the injection yielding the best results in terms of range extension, which corresponds to the injection yaw angle of −30 deg case, leads to an incidence of about 0 deg over the tip. This situation is depicted in Fig. 10c. Comparing Fig. 10c, which shows the injection YA of −30 deg case, to other injection cases shows that the best injection pushes the shock further backward relative to the blade leading edge than any other case. Therefore, a relatively smaller zone of negative axial velocity is formed downstream of the shock for this case.

As discussed earlier, stall occurs when the diffusion factor at 98% span reaches a value of about 0.75, regardless of the injection configuration. Figure 11 shows the static pressure contours together with the relative velocity vectors at 98% span for the smooth casing, the axial injection, and the injection YA of −30 deg case at their respective near-stall points. The bold lines denote zero axial velocity contour levels. For all the cases, the passage shock is detached from the blade leading edge. It is further shown that the tip leakage vortex moves radially inward and appears in the plot as a negative axial velocity zone and also a low-static pressure region along the suction surface near the blade leading edge.

Unsteady calculations were conducted for the smooth casing and the injection YA of −30 deg case to identify the effects of unsteadiness on the results. Figure 12 shows the static pressure contours at the tip section and the near-stall point for the smooth casing. The zero axial velocity contour levels were also added to the plots. Figure 12a corresponds to the steady simulations, whereas Fig. 12b shows the time-averaged contours (averaged over 600 time steps) from the unsteady calculations. Similar contour plots are shown in Figs. 13a and 13b for the injection YA of −30 deg case at its near-stall point. Comparing the steady and unsteady results shows a further movement of the shock upstream of the passage in the time-averaged contour plots. It is further shown that the unsteady simulations predict a larger zone of negative axial velocity fluid near the tip of the blade, which is due to the shock motion and vortex shedding. Comparing Figs. 12 and 13 shows that the effect of unsteadiness is more pronounced for the injection case, which is operating at a lower mass flow rate.

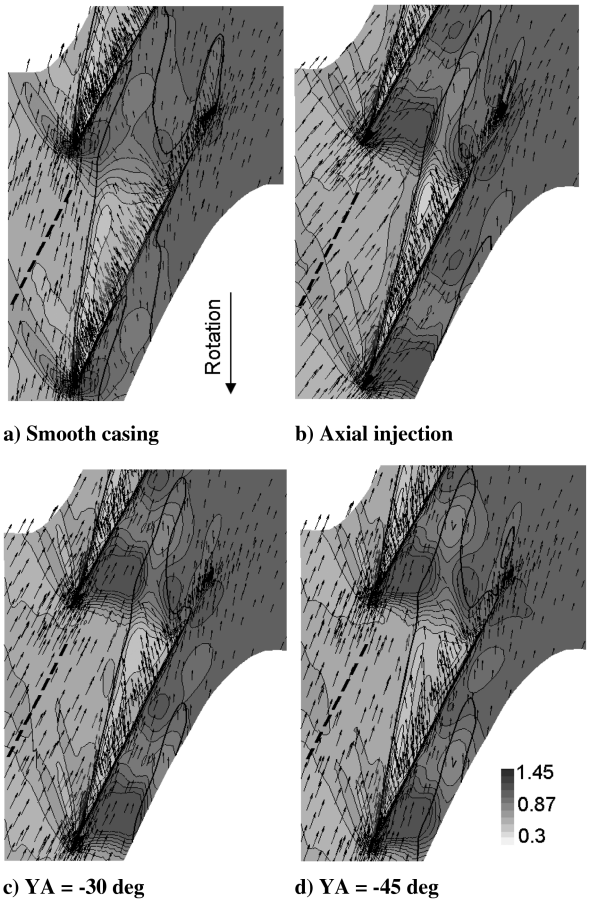

Fig. 10 Static pressure contours at 99.6% span and the stalling mass flow of the smooth casing.

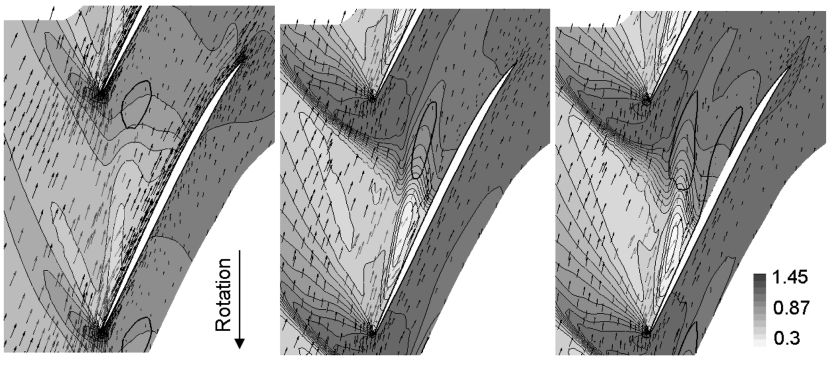

Fig. 11 Static pressure contours at 98% span and the near-stall point of each case.

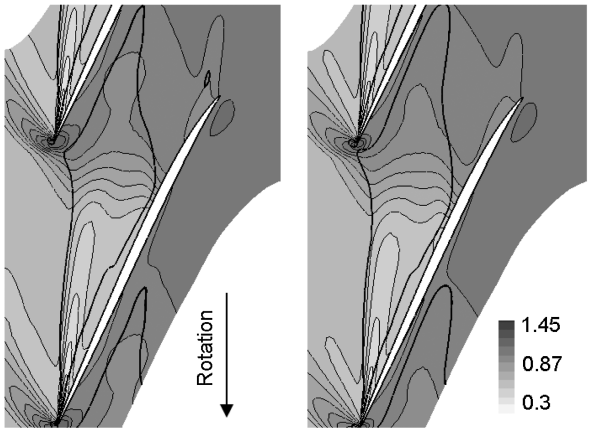

a) Steady calculations b) Time-averaged result

Fig. 12 Static pressure contours for the smooth casing at the tip and the near-stall point.

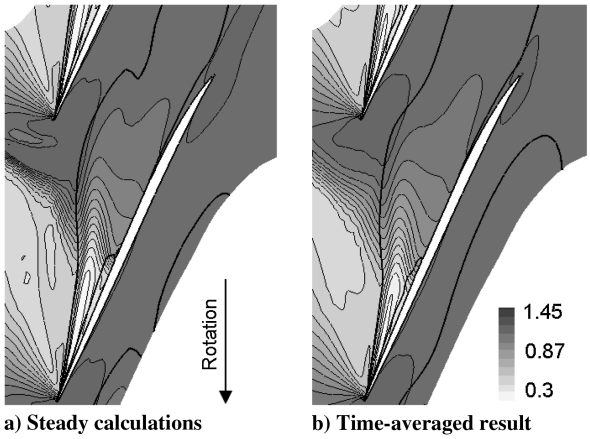

a) Steady calculations b) Time-averaged result

Fig. 13 Static pressure contours for the injection YA of −30 deg case at the tip and the near-stall point.

V. Conclusions

The numerical simulations were performed on a NASA Rotor-67 with and without tip injection. A parametric study of the effect of the injection angle on the compressor stability was carried out. The following observations and conclusions were obtained:

1) Mass injection improves the compressor stability by unloading the tip of the blade. It was found that stall occurs when the diffusion factor at around 98% span exceeds a value of about 0.75.

2) Injection angle is found to play an important role in the compressor stability. Injection with pitch or positive yaw angles reduces the compressor stability as compared with the axial injection case.

3) Range extension can be related to an increase in the momentum due to the injection, which is evaluated in the relative frame of reference.

4) The flowfield in the vicinity of the casing is subject to Coanda effects in the cases in which the injection has a pitch angle. For these cases, the axial velocity components of the injected air passing over the tip of the blade are lower than when the injection is purely axial.

5) Tip injection pushes the shock backward in the passage and reduces the region of negative axial velocity near the tip of the blade. The best injection case was found to correspond to a negative yaw angle (−30 deg). This injection angle creates an incidence of about 0 deg over the tip and adds the highest momentum in the relative frame of reference. In this condition, the passage shock is pushed further downstream relative to all other injection cases. This injection benefits the stability by some 32% as compared with the axial injection.

Combinations of the pitch and yaw angles were not studied in this paper. However, it is expected that using a pitch angle together with the yaw angle cases would reduce the stability, owing to the ensuing Coanda effect.

Acknowledgments

The authors gratefully acknowledge the British Council and Iranian Ministry of Science, Research, and Technology for their support. The authors would also like to thank Chris Freeman for his helpful comments regarding this work. Special thanks are due to Pericles Pilidis from Cranfield University for the support he offered to the first author.

References

[1] Vo, H. D., Tan, C. S., and Greitzer, E. M., "Criteria for Spike Initiated Rotating Stall," American Society of Mechanical Engineers Paper GT2005-68374, 2005.

[2] Hah, C., Bergner, J., and Schiffer, H. P., "Short Length-Scale Rotating Stall Inception in a Transonic Axial Compressor—Criteria and Mechanisms," American Society of Mechanical Engineers Paper GT2006-90045, 2006.

[3] Davis, R. L., and Yao, J., "Axial Compressor Rotor Flow Structure at Stall-Inception," AIAA Paper 2006-419, 2006.

[4] Schlechtriem, S., and Loetzerich, M., "Breakdown of Tip Leakage Vortices in Compressors at Flow Conditions Close to Stall," American Society of Mechanical Engineers Paper 97-GT-41, 1997.

[5] Suder, K. L., and Celestina, M. L., "Experimental and Computational Investigation of the Tip Clearance Flow in a Transonic Axial Compressor Rotor," *Journal of Turbomachinery*, Vol. 118, No. 2, 1996, pp. 218–229.

[6] Adamczyk, J. J., Celestina, M. L., and Greitzer, E. M., "The Role of Tip Clearance in High-Speed Fan Stall," *Journal of Turbomachinery*, Vol. 115, No. 1, 1993, pp. 28–39. doi:10.1115/1.2929212

[7] Puterbaugh, S. L., and Brendel, M., "Tip Clearance Flow-Shock Interaction in a Transonic Compressor Rotor," *Journal of Propulsion and Power*, Vol. 13, No. 1, 1997, pp. 24–30.

[8] Hah, C., Rabe, D. C., and Wadia, A. R., "Role of Tip-Leakage Vortices and Passage Shock in Stall Inception in a Swept Transonic Compressor Rotor," American Society of Mechanical Engineers Paper GT2004-53867, 2004.

[9] Copenhaver, W. W., Puterbaugh, S. L., and Hah, C., "Unsteady Flow and Shock Motion in a Transonic Compressor Rotor," *Journal of Propulsion and Power*, Vol. 13, No. 1, 1997, pp. 17–23.

[10] Prince, D. C., Jr., Wisler, D. C., and Hivers, D. E., "Study of Casing Treatment Stall Margin Improvement Phenomena," NASA CR-134552, 1974.

[11] Crook, A. J., Greitzer, E. M., Tan, C. S., and Adamczyk, J. J., "Numerical Simulation of Compressor Endwall and Casing Treatment Flow Phenomena," *Journal of Turbomachinery*, Vol. 115, No. 3, 1993, pp. 501–512. doi:10.1115/1.2929280

[12] Shabbir, A., and Adamczyk, J. J., "Flow Mechanism for Stall Margin Improvement Due to Circumferential Casing Grooves on Axial Compressors," *Journal of Turbomachinery*, Vol. 127, No. 4, 2005, pp. 708–717. doi:10.1115/1.2008970

[13] Wisler, D. C., and Beacher, B. F., "Improved Compressor Performance Using Recessed Clearance (Trenches)," *Journal of Propulsion and Power*, Vol. 5, No. 4, 1989, pp. 469–475. doi:10.2514/3.23178

[14] Freeman, C., Wilson, A. G., Day, I. J., and Swinbanks, M. A., "Experiments in Active Control of Stall on an Aeroengine Gas Turbine," *Journal of Turbomachinery*, Vol. 120, No. 4, 1998, pp. 637–647.

[15] Hathaway, M. D., "Self-Recirculating Casing Treatment Concept for Enhanced Compressor Performance," NASA TM-2002-211569, 2002.

[16] Strazisar, A. J., Bright, M. M., Thorp, S., Culley, D. E., and Suder, K. L., "Compressor Stall Control Through Endwall Recirculation," American Society of Mechanical Engineers Paper GT2004-54295, 2004.

[17] Epstein, A. H., Ffowcs Williams, J. E., and Greitzer, E. M., "Active Suppression of Aerodynamic Instabilities in Turbomachines," *Journal of Propulsion and Power*, Vol. 5, No. 2, 1989, pp. 204–211. doi:10.2514/3.23137

[18] Day, I. J., "Active Suppression of Rotating Stall and Surge in Axial Compressors," *Journal of Turbomachinery*, Vol. 115, No. 1, 1993, pp. 40–47. doi:10.1115/1.2929216

[19] Schobeiri, M. T., and Attia, M., "Active Control of Compressor Instability and Surge by Stator Blades Adjustment," *Journal of Propulsion and Power*, Vol. 19, No. 2, 2003, pp. 312–317.
[20] Paduano, J., Epstein, A., Valvani, L., Longley, J., Greitzer, E., and Guenette, G., "Active Control of Rotating Stall in a Low-Speed Axial Compressor," *Journal of Turbomachinery*, Vol. 115, No. 1, 1993, pp. 48–56.
doi:10.1115/1.2929217
[21] Eveker, K. M., Gysling, D. L., Nett, C. N., and Sharma, O. P., "Integrated Control of Rotating Stall and Surge in High-Speed Multistage Compression Systems," *Journal of Turbomachinery*, Vol. 120, No. 3, 1998, pp. 440–445.
[22] Yeung, S., Wang, Y., and Murray, R. M., "Bleed Valve Rate Requirements Evaluation in Rotating Stall Control on Axial Compressors," *Journal of Propulsion and Power*, Vol. 16, No. 5, 2000, pp. 781–791.
[23] Niazi, S., Stein, A., and Sankar, L. N., "Numerical Studies of Stall and Surge Alleviation in a High-Speed Transonic Fan Rotor," AIAA Paper 2000-0225, 2000.
[24] Spakovszky, Z. S., Weigl, H. J., Paduano, J. D., Van Schalkwyk, C. M., Suder, K. L., and Bright, M. M., "Rotating Stall Control in a High-Speed Stage with Inlet Distortion: Part I—Radial Distortion," *Journal of Turbomachinery*, Vol. 121, No. 3, 1999, pp. 510–516.
[25] Weigl, H. J., Paduano, J. D., Frechette, L. G., Epstein, A. H., Greitzer, E. M., Bright, M. M., and Strazisar, A. J., "Active Stabilization of Rotating Stall and Surge in a Transonic Single Stage Axial Compressor," *Journal of Turbomachinery*, Vol. 120, No. 4, 1998, pp. 625–636.
[26] Koch, C. C., and Smith, L. H., Jr., "Experimental Evaluation of Outer Casing Blowing or Bleeding of Single Stage Axial Flow Compressor, Part 4: Performance of Bleed Insert Configuration No. 3," NASA CR-54590, 1968.
[27] Lee, N. K. W., and Greitzer, E. M., "Effects of Endwall Suction and Blowing on Compressor Stability Enhancement," *Journal of Turbomachinery*, Vol. 112, No. 1, Jan. 1990, pp. 133–144.
doi:10.1115/1.2927410
[28] Suder, K. L., Hathaway, M. D., Thorp, S. A., Strazisar, A. J., and Bright, M. B., "Compressor Stability Enhancement Using Discrete Tip Injection," *Journal of Turbomachinery*, Vol. 123, No. 1, 2001, pp. 14–23.
doi:10.1115/1.1330272
[29] Stein, A., Niazi, S., and Sankar, L. N., "Computational Analysis of Stall and Separation Control in Centrifugal Compressors," *Journal of Propulsion and Power*, Vol. 16, No. 1, 2000, pp. 65–71.
[30] Hendricks, G., and Gysling, D., "Theoretical Study of Sensor-Actuator Schemes for Rotating Stall Control," *Journal of Propulsion and Power*, Vol. 10, No. 1, 1994, pp. 101–109.
doi:10.2514/3.23717
[31] Buhr, C. A., Franchek, M. A., and Fleeter, S., "Rotating Stall Control in Axial Compressor Subject to Wheel Speed Transients," *Journal of Propulsion and Power*, Vol. 22, No. 2, 2006, pp. 404–410.
doi:10.2514/1.6272
[32] Chen, J., Webster, R., Hathaway, M. D., Herrick, G. P., and Skoch, G. J., "Numerical Simulation of Stall and Stall Control in Axial and Radial Compressors," AIAA Paper 2006-418, 2006.
[33] Sheng, C., and Remotigue, M., "Numerical Simulation of Rotor 35 with and Without Tip Injection Using an Arbitrary Mach Number Flow Solver," AIAA Paper 2004-372, 2004.
[34] Beheshti, B. H., Farhanieh, B., Ghorbanian, K., Teixeira, J. A., and Ivey, P. C., "Performance Enhancement in Transonic Axial Compressors Using Blade Tip Injection Coupled with Casing Treatment," *Proceedings of the Institution of Mechanical Engineers. Part A, Journal of Power and Energy*, Vol. 219, No. 5, 2005, pp. 321–331.
doi:10.1243/095765005X28607
[35] Strazisar, A. J., Wood, J. R., Hathaway, M. D., and Suder, K. L., "Laser Anemometer Measurements in a Transonic Axial-Flow Fan Rotor," NASA TP-2879, 1989.
[36] Khaleghi, H., Tousi, A. M., Boroomand, M., and Teixeira, J. A., "Recirculation Casing Treatment by Using a Vaned Passage for a Transonic Axial-Flow Compressor," *Proceedings of the Institution of Mechanical Engineers. Part A, Journal of Power and Energy*, Vol. 221, No. 8, 2007, pp. 1153–1162.
doi:10.1243/09576509JPE444
[37] Chima, R. V., "Calculation of Tip Clearance Effects in a Transonic Compressor Rotor," *Journal of Turbomachinery*, Vol. 120, No. 1, 1998, pp. 131–140.
[38] Hah, C., and Reid, L., "A Viscous Flow Study of Shock-Boundary Layer Interaction, Radial Transport, and Wake Development in a Transonic Compressor," *Journal of Turbomachinery*, Vol. 114, No. 3, July 1992, pp. 538–547.
doi:10.1115/1.2929177
[39] Khaleghi, H., Boroomand, M., Teixeira, J. A., and Tousi, A. M., "A Numerical Study of the Effects of Injection Velocity on Stability Improvement in High-Speed Compressors," *Proceedings of the Institution of Mechanical Engineers. Part A, Journal of Power and Energy*, Vol. 222, No. 2, 2008, pp. 189–198.
doi:10.1243/09576509JPE443

F. Liu
Associate Editor